Enhanced Direct White Light Emission Efficiency in Quantum Dot Light-Emitting Diodes via Embedded Ferroelectric Islands Structure

Yuljae Cho,* Sangyeon Pak, Benxuan Li, Bo Hou, SeungNam Cha*

Dr. Yuljae Cho
University of Michigan – Shanghai Jiao Tong University Joint Institute, Shanghai Jiao Tong University, 800 Dong Chuan Road, Minghang District, Shanghai 200240, China
Email: yuljae.cho@sjtu.edu.cn

Dr. Sangyeon Pak, Prof. SeungNam Cha
Department of Physics, Sungkyunkwan University, 2066, Seobu-ro, Jangan-gu, Suwon, Gyeonggi-do, 16419 Republic of Korea
Email: chasn@skku.edu

Dr. Benxuan Li
Department of Engineering, University of Cambridge, 9 JJ Thomson Avenue, Cambridge CB3 0FF, UK

Prof. Bo Hou
School of Physics and Astronomy, Cardiff University, 5 The Parade, Newport Road, Cardiff, CF24 3AA, United Kingdom

Abstract

White light emission is of great importance in our daily life as it is the primary source of light indoor and outdoor as well as day and night. Among various materials and lighting technologies, intensive efforts have been made to quantum dots based-light-emitting diode (QLEDs) because of outstanding optical properties, facile synthesis, and bandgap tunability of QDs. Despite the fact that QLEDs are able to present various colors in a visible range, realizing efficient direct white light emission has been a challenge as white light emission can only be achievable through stacking and patterning of QD films or mixing of different sizes of QDs. This inevitably involves energy band mismatch at interfaces, leading to degradation of device performance. Here, we introduce a new effective method to improve white QLED performances through embedding a ferroelectric islands structure which induces an electric field to effectively modulate the energy band at the junction interface. The formation of favorable energy landscape leads to efficient charge transport, improved radiative recombination, and consequently high EQE in the white QLEDs. In addition, we demonstrate that our new approach is proved to be effective in different color temperature ranging from 3000 to over 120,000 Kelvin.

Introduction

In 2014, Nobel prize was given to researchers who invented gallium nitride (GaN)-based blue light emitting diodes (LEDs). This opened up great advancement in white light emission, which contributed to saving massive amount of energy as one fourth of electricity is being consumed for the lighting purpose over the world.[1] Ever since, tremendous research efforts

2

have been paid to improve the efficiency of white LEDs.[2-9] However, white light emission was mostly achieved by wavelength conversion because direct white light emission required the LEDs to simultaneously emit different color spectra. Therefore, over the past decades, synthesis of the active materials with the appropriate bandgaps was one of the major challenges to achieve direct white light emission.

Colloidal quantum dots (QDs), in particular, cadmium selenide-zinc sulfide core shell QDs (CdSe@ZnS), are considered to be the prospective active materials in lightings and displays as they possess outstanding optical properties, such as color tunability, narrow emission width, high photoluminescence quantum yield (PLQY), high stability, and solution-processability for facile fabrication.[10-13] The QDs can be driven electrically in QD-LEDs (in short, QLEDs hereafter) and they have demonstrated high brightness, high external quantum efficiency (EQE), device stability, and low power consumption.[14-18] In particular, white QLEDs have attracted considerable attention because the QDs are technologically favorable to achieve direct white light emission by simply mixing red (R), green (G), and blue (B) color QDs.[19-22] More importantly, for future displays with high definition, industries have put intensive efforts in integrating white light into a pixel together with RGB. The solution processability of the mixed white QD provides cost-effective and facile fabrication process, which is attractive and desirable to industrial applications. Nevertheless, the existence of different sizes of QDs in a mixed RGB QD solution can limit the overall performance of white QLEDs due to the difficulties in predicting the energy band alignments that govern charge balance, radiative recombination, and driving current. This has limited to develop an

effective method to improve the performance of a white QLED. As a result, a new universal approach is required to add a driving force to tailor the energy band alignment so that charge transport and luminescence within the LEDs can be improved to achieve high performance in direct white light emission and high resolution in future display technology.

Here, we introduce a ferroelectric islands layer using poly(vinylidene fluoride-trifluoroethylene), P(VDF-TrFE), to effectively modulate energy band levels and induce an additional electric field which facilitates charge carrier transport. This structural modification provides direct white light emission via a much simpler way to fabricate white LEDs with higher device performance. In addition, our new method is applicable to devices with different color temperature for direct white light emission without a wavelength conversion. White QLEDs with the P(VDF-TrFE) islands layer exhibit 37 and 48% improvement in EQE compared to reference devices for warm white and daylight white color, respectively. In addition, we demonstrate universality of our new method in various white color temperatures ranging from 3,000 to 120,000 Kelvin (K), corresponding to from warm to cool white color. The white QLEDs with different color temperatures all exhibit significant improvement in device performances, which suggests that our new method is a facile and effective way to enhance direct white light emission efficiency.

Results and Discussion

Figure 1(a) illustrates the structure of a ferroelectric effect QLED (FE-QLED), consisting of indium tin oxide (ITO), poly(3,4-ethylenedioxythiophene) polystyrene sulfonate

4

(PEDOT:PSS), Poly(9,9-dioctylfluorene-alt-benzothiadiazole) (TFB), CdSe/ZnS QDs, zinc oxide nanoparticles (ZnO NPs), and aluminum (Al) electrode where P(VDF-TrFE) is deposited either between the TFB and QD layer or between the QD and ZnO NP layer. To fabricate a FE-QLED, we used a spin-coating method to demonstrate the solution processability of the FE-QLED (details of fabrication method are shown in Methods). As the transmission electron microscopy (TEM) cross sectional image of the FE-QLED shows in Figure 1(b), the thickness of each layer was approximately 45 nm for both PEDOT:PSS and TFB, 15 nm for CdSe/ZnS QDs, and 30 nm for ZnO NPs. The TEM image in Figure 1(c) shows RGB mixed CdSe/ZnS QDs in a ratio of 1:2:9 without any aggregation where the photoluminescence quantum yield (PLQY) of red, green, and blue QDs was 84%, 81%, and 83%, respectively. Figure 1(d) shows PL characteristics of the RGB mixed QD solution with 75% PLQY, exhibiting three distinct wavelengths at ~625 nm, ~525 nm, and ~450 nm. A slight decrease in PLQY of the mixed QD solution compared to the PLQY of each RGB QD solution is due to Förster resonance energy transfer (FRET) from large bandgap QDs to small bandgap QDs, namely from blue to green and red light emissive QDs.[21-25] This phenomenon becomes more apparent by exhibiting the decrease in the PLQY in the QD film where the distance between QDs is reduced as shown in Figure S1 in Supporting Information (SI).[26] The PL characteristics of QD films showed an opposite trend compared to those of the QD solutions: the intensity of PL in the films is $I_{red} > I_{green} \approx I_{blue}$ whereas the PL intensity in the solutions is $I_{blue} > I_{green} \approx I_{red}$. This resulted from the increased FRET process in the film state due to reduced distance between QDs.[23,27] As a result, a much higher volume of blue QDs

5

were required than that of green and red QDs in the mixed QD solution for white light emission evidenced by the RGB mixing ratio 1:2:9, which is well consistent with previous reports that employed larger fraction of the QDs with higher bandgap than the QDs with lower bandgap.[19,23,28]

For a ferroelectric layer, we employed ferroelectric polymer P(VDF-TrFE) due to the fascinating material properties of P(VDF-TrFE), such as chemical inertness, low fabrication temperatures, photostability, and its large electric polarization at even one nanometer thickness.[29,30] Ferroelectric P(VDF-TrFE) polymer was directly deposited on either the TFB or QD layer. Well-distributed P(VDF-TrFE) islands were formed when it was spin-casted on both films as shown in Figure 1(e) and Figure S2(a) and (b) in SI, which is due to the similar surface energy of the TFB and QD layer as indicated by the contact angle (Figure S3 in SI). The size and coverage of the P(VDF-TrFE) island structure on TFB and QD layer was controlled by employing either spin-coating or spin-casting method as well as changing the concentration of P(VDF-TrFE) solutions and the optimum condition was attained at the concentration of 0.2 wt% with the spin-casting method as shown in Figure S4 in SI. The average height of the P(VDF-TrFE) islands was approximately 7 nm as shown in Figure S2(c) in SI. It is worth noting that P(VDF-TrFE) does not absorb light in the visible range due to its high bandgap, ~ 6 eV, which holds the same for the ZnO layer (~3.4 eV).[31,32] As shown in Figure S5 in SI, the transmittance of the P(VDF-TrFE) and P(VDF-TrFE) on the ZnO layer in the visible range was almost similar, which demonstrates that there was negligible light reflection from the P(VDF-TrFE) islands structures. In order to confirm the

6

ferroelectric properties of the islands layer, X-ray diffraction (XRD) was performed and monitored its distinctive peaks. As shown in Figure 1(f), the P(VDF-TrFE) islands layer deposited on the ZnO/ ITO layer exhibited the peak near $2\theta \sim 20°$, indicating that the P(VDF-TrFE) islands layer formed the β-phase, i.e., a ferroelectric phase.[30] To further confirm that the island structures are formed by the P(VDF-TrFE) solution, we further analyzed X-ray photoelectron spectra (XPS). Figure S6(a) shows four prominent C states in C 1s deconvoluted spectra: ~ 284.50 eV of organic contaminants, ~ 286.00 eV of saturated hydrocarbon CH_2, ~ 288.40 eV of C–F–H, and ~ 290.50 eV of CF_2. In addition, F 1s spectrum with the peak position ~ 687.40 eV was identified in Figure S6(b).[33,34] These results indicate that the island structure is formed by coating the P(VDF-TrFE) solution.

When negative and positive voltages are applied to the Al and ITO electrodes, respectively, electric dipoles are aligned in a way that negative charges to the ITO side and positive charges to the Al side in the β-phase P(VDF-TrFE) layer, which modulates local energy band levels near the P(VDF-TrFE) layer. By judiciously using this phenomenon, we observed significant enhancement in the QLED performances, which will be discussed shortly.

Figure 2 illustrates the schematics of energy band diagram in three different types of QLEDs used in this study. The energy level of each layer was referred to literature reported previously.[20,21] We define each FE-QLED with respect to the location of P(VDF-TrFE) islands layer as follows: (1) a reference device without the P(VDF-TrFE) layer (Figure 2(a)

7

and (d)); (2) a T/Q FE-QLED with the P(VDF-TrFE) layer between the TFB and QD layer (Figure 2(b) and (e)); and (3) a Q/Z FE-QLED with the P(VDF-TrFE) between the QD and ZnO layer (Figure 2(c) and (f)), respectively. At low forward bias (Figure 2(a)-(c)), electric dipoles in the P(VDF-TrFE) islands layer start aligning towards negative to ITO (anode) and positive to Al (cathode). Due to the low forward bias condition, a dipole polarization field is relatively weaker than the polarization field at high forward bias condition (Figure 2(e) and (f)). As a result, energy levels near the P(VDF-TrFE) islands layer are slightly bent whereas the reference cell does not show any band bending effect as shown in Figure 2(a)-(c).

When higher potential is applied to the QLEDs, there are two mechanisms causing energy band shift: (1) shift of conduction and valence levels of the TFB and ZnO layers by the applied bias; and (2) the energy band bending at the edge between the TFB and QD layer (Figure 2(e)) or between the QD and ZnO layer (Figure 2(f)) due to the ferroelectric field of the P(VDF-TrFE) layer. As shown in Figure 2(f), the energy band bending in the Q/Z FE-QLED is favorable for electron transport, and therefore, charge carrier transport is facilitated in this device structure. However, the T/Q FE-QLED (Figure 2(e)) forms a higher barrier for holes at the interface between the TFB and the QD layer, which limits the efficient transport of charge carriers. Moreover, the energy band bending in the T/Q FE-QLED (Figure 2(e)) causes a leakage current and consequently non-radiative recombination at the TFB and QD interface due to the proximity of energy levels between the valence level of TFB and the conduction level of the QDs, leading to the degraded device performance.

8

To confirm our conjecture, we characterized the performance of each device type. **Figure 3** illustrates the device characteristics of warm and daylight white FE-QLEDs where the terms, warm and daylight white, were used based on the color temperature of the device.[35] As it was predicted, the device performance was modulated depending on the existence of the P(VDF-TrFE) islands layer and its inserted location in the device. All the devices were measured by applying from low to high potentials to effectively investigate the dipole polarization effect in the QLEDs.[36-38] For both warm and daylight white Q/Z FE-QLEDs (Figure 2(c) and (f)), higher luminance (approximately 20% and 30% improvement, respectively) and EQE (approximately 37% and 48% improvement, respectively) were observed compared to the reference cells as shown in Figure 3(a) and Table 1. It is worth noting that the turn-on voltage (V_{on}) of the Q/Z device was 0.1 V higher than that of the T/Q one (Table 1). This is because of a notch formed between the conduction band level of QD and ZnO layer at the low applied bias condition (Figure 2(c)). The significant enhancement in the device performance is attributed to the energy band level modification by the dipole polarization of the P(VDF-TrFE) islands layer, constructing a favorable energy band structure for the efficient charge carrier transport as well as increased radiative recombination. In addition, the FE-QLEDs exhibited high long-term stability, maintaining 90 % of the L/L0 ratio with an initial luminance (L0) of ~ 1000 cd/m^2 for more than 250 min as shown in Figure S7 in SI. QLEDs were encapsulated using an epoxy and a glass coverslip. Measurement was conducted in ambient air condition at room temperature. On the contrary, increased leakage current was observed in the T/Q FE-QLEDs as shown in Figure S8 and S9

9

in SI, which is due to the lowered energy level difference between the valence band level of TFB and conduction band level of QDs caused by the electric dipoles. This led to the inefficient charge carrier transport and accordingly higher rates of non-radiative recombination. As a result, both luminance and EQE of the devices were deteriorated. Details of device performance are shown in Figure S8, S9, and Table 1. It is worth noting that there is a trade-off between the induced ferroelectric field and more coverage of the P(VDF-TrFE) layer on either TFB or QD layer due to the insulating nature of P(VDF-TrFE). Therefore, the introduction of the P(VDF-TrFE) island structure is crucial to open an enough channel for charges to be transported (Figure S4 in SI). In addition, the height of P(VDF-TrFE) was carefully controlled for our study so that the P(VDF-TrFE) island structure did not penetrate through the layer deposited on it.

Figure 3(b) and (e) show the distinct EL characteristics of the Q/Z devices for warm and daylight white devices, respectively. Correlated color temperature (CCT) at maximum luminance (at 8 V of applied bias) was found to be 3000K for the warm white and 6500K for daylight white QLED. Interestingly, to tune the color temperature, far larger amount of blue QDs were needed: for warm white, the ratio of RGB QDs was 1:3.5:3.5 whereas RGB ratio was 1:2:9 for daylight white emission. This is due to the FRET from blue to green and red QDs, which is well consistent with the PLQY measurement, i.e. when the mixed QDs formed a QD layer, PLQY of blue QDs significantly decreased as FRET increased due to the reduced dot-to-dot distance which was discussed in Figure 1.[21-26,28] However, the severe imbalance of the RGB ratio leads to degradation of white QLED performance because a turn-on voltage

10

of a QLED would increase due to the high ratio of blue QDs with the larger bandgap as evidenced by the turn-on voltage of warm and daylight white QLEDs in Table 1. Therefore, smaller amount of blue QDs is desirable with the same CCT value. In this regard, for daylight white emission, we employed QDs with a deep blue color, or shorter wavelength, to avoid performance degradation. Commission internationale de l'éclairage (CIE) chromaticity is shown in Figure 3(c) and (f) where CIE coordinate for warm and daylight white was found to be (0.4473, 0.4165) and (0.3151, 0.3039) at maximum luminance, respectively. Gradual color modulation from red to white color in CIE chromaticity was observed as the applied potential increased.

To demonstrate the universality of our new approaches for enhanced white light emission, white QLEDs with various CCT values with and without the ferroelectric islands layer were fabricated. The details of RGB mixing ratio are shown in Table S1 in SI. **Figure 4(a)** illustrates EQE improvement of various FE-QLEDs where higher CCT values indicate that the light emission includes higher portion of blue light. Luminance-EQE plots and EL characteristics are shown in S10-S12 in SI and device parameters are summarized in Table S2 in SI. It was found that the improvement in EQE was more prominent in devices with higher CCT values. We ascribed this to larger amount of surface traps in blue QDs due to the high surface area to volume ratio than those of red and green QDs.[39,40] Because larger amount of blue QDs was required to have higher CCT values as shown in Table S1, the RGB mixed QD solution with more blue QDs have more surface traps that lead to non-radiative

recombination, deteriorating intensity of light emission, power efficiency, and EQE.[41-44] This phenomenon was also observed in PLQY measurement of the mixed QD solutions with higher volume ratio of blue QDs. As shown in Figure S13, addition of blue QDs to the mixed solution exhibited relatively small increase in PL at blue wavelength whereas decrease in PL at green and red were noticeable, which led to decrease in PLQY from 26.35% to 24.14%. Therefore, the EQE improvement was more prominent in devices with higher CCT values by the employment of P(VDF-TrFE) layer which facilitated charge carrier transport and consequently reducing non-radiative recombination at the surface traps in small size blue QDs. Corresponding CIE coordinates were marked in the Figure 4(b), demonstrating the universality of the ferroelectric effect-enhanced QLEDs performance for direct white light emission with various color temperatures. Finally, performances of white QLEDs in this work were compared with other works reported in recent 10 years as shown in Table S3 in Si.

In summary, we have demonstrated an enhanced direct white light emission by judiciously employing a ferroelectric polymer P(VDF-TrFE) islands layer. Electric dipoles in the embedded P(VDF-TrFE) layer were polarized by the application of bias, which resulted in energy band bending at the local area. Favorable energy band bending, formed by the P(VDF-TrFE) layer between QD and ZnO layer, facilitated charge carrier transport and consequently enhanced device performance with high luminance. Our new strategy further demonstrated its versatile ability to improve performances of white QLEDs with different CCT values, ranging from warm to cool temperature. The facile but effective and versatile

12

new approach would bring great opportunities in advancing direct white light emission which

is necessary for pursuing our daily lives.

Author Manuscript

Methods

Material preparation: Pixelated ITO substrates, PEDOT:PSS solution and TFB powder were purchased from Ossila. CdSe@ZnS QDs were synthesized following previous works with some modifications.[45,46] ZnO nanoparticles (NPs) were synthesized using previously reported recipe by our group.[47,48] Pixelated ITO substrates were cleaned using acetone, 1-propanol, and warm deionized water for 10 minutes, respectively. Cleaned ITO substrates were dried by blowing nitrogen, and then, UV-Ozone treatment was carried out on the substrates for 5 minutes. A concentration of a TFB, P(VDF-TrFE), CdSe/ZnS QDs, and ZnO NPs solution was 8 mgml^{-1}, 0.2 wt%, 12.5 mgml^{-1}, and 25 mgml^{-1}, respectively.

Device fabrication: PEDOT:PSS was spin-coated at the speed of 3000 rpm for 45 seconds and then baked at 150 °C in ambient air for 20 minutes. After the annealing, the PEDOT:PSS coated substrates were transferred to a nitrogen-filled glove box, and then annealed again at 150 °C for 15 minutes. TFB (8 mgml^{-1}) in chlorobenzene was spin-coated on the PEDOT:PSS layer at the speed of 4000 rpm for 45 seconds, which was followed by thermal annealing at 130 °C for 30 minutes. CdSe@ZnS QDs (12.5 mgml^{-1}) in hexane were spin-casted on the TFB layer at a speed of 4000 rpm for 30 seconds, and then thermally annealed at 90 °C for 10 minutes. ZnO NPs (25 mgml^{-1}) in ethanol were spin-coated on the QD layer at the speed of 3000 rpm for 30 seconds, which was followed by thermal annealing at 80 °C for 10 minutes. P(VDF-TrFE) (0.2 wt%) in 2-bunatone was spin-casted on either TFB layer or QD layer at 4000 rpm for 30 seconds. Then, thermal annealing was performed to form β-

14

phase at 130 °C for 20 minutes. Finally, Al electrode (100 nm) was deposited using a thermal evaporator. The active area of a QLED was 0.045 cm^2.

Device characterization: All QLEDs were passivated in the glove box after deposition of the Al electrode, and then, measurements were performed using HAMAMATSU PMA-12 connected with Keithley 2400 source meter. The cross-sectional TEM images of the QLEDs were characterized by a high-resolution (HR)-STEM (FEI Tecnai F20 FEGTEM), and the samples were sliced using a focused ion beam (FIB) system (Dual-Beam FIB, FEI Helios Nanolab SEM/FIB).

Declaration of Competing Interest

The authors declare that they have no known competing financial interests or personal relationships that could have appeared to influence the work reported in this paper.

Acknowledgement

Author Contributions

Y.C. and S.P. fabricated devices and performed materials as well as device characterizations. B.H. synthesized materials. B.L. performed contact angle measurement. The manuscript was written by Y.C., S.P., and S.C. and revised by all authors.

Appendix A. Supporting information

Supplementary data associated with this article can be found in the online version.

References

[1] Y. Nanishi, *Nat. Photon.* **2014**, *8*, 884.

[2] S. Pimputkar, J. S. Speck, S. P. DenBaars, S. Nakamura, *Nat. Photon.* **2009**, *3*, 180.

[3] H. Jia, L. Guo, W. Wang, H. Chen, *Adv. Mater.* **2009**, *21*, 4641.

[4] E. Jang, S. Jun, H. Jang, J. Lim, B. Kim, Y. Kim, *Adv. Mater.* **2010**, *22*, 3076.

[5] K. Kim, J. Y. Woo, S. Jeong, C. -S. Han, *Adv. Mater.* **2011**, *23*, 911.

[6] H. Zhang, Q. Su, S. Chen, *Nat. Commun.* **2020**, *11*, 2826.

[7] X. Dai, Z. Zhang, Y. Jin, Y. Niu, H. Cao, X. Liang, L. Chen, J. Wang, X. Peng, *Nature* **2014**, *515*, 96.

[8] Q. Lin, L. Wang, Z. Li, H. Shen, L. Guo, Y. Kuang, H. Wang, L. S. Li, *ACS Photonics* **2018**, *5*, 939.

[9] K. Ding, H. Chen, L. Fan, B. Wang, Z. Huang, S. Zhuang, B. Hu, L. Wang, *ACS Appl. Mater. Interfaces* **2017**, 9, 20231.

[10] X. -B. Li, C. -H. Tung, L. -Z. Wu, *Nat. Rev. Chem.* **2018**, *2*, 160.

[11] M. Yuan, M. Liu, E. H. Sargent, *Nat. Energy* **2016**, *1*, 16016.

[12] H. Shen, Q. Lin, H. Wang, L. Qian, Y. Yang, A. Titov, J. Hyvonen, Y. Zheng, L. S. Li, *ACS Appl. Mater. Interfaces* **2013**, *5*, 12011.

[13] H. Shen, Q. Gao, Y. Zhang, Y. Lin, Q. Lin, Z. Li, L. Chen, Z. Zeng, X. Li, Y. Jia, S. Wang, Z. Du, L. S. Li, Z. Zhang, *Nat. Photon*. **2019**, *13*, 192.

[14] J. Song, O. Wang, H. Shen, Q. Lin, Z. Li, L. Wang, X. Zhang, L. S. Li, *Adv. Funct. Mater.* **2019**, *29*, 1808377.

[15] M. Ban, Y. Zou, J. P. Rivett, Y. Yang, T. H. Thomas, Y. Tan, T. Song, X. Gao, D. Credington, F. Deschler, *Nat. Commun.* **2018***, 9,* 3892.

[16] Z. Zhang, Y. Ye, C. Pu, Y. Deng, X. Dai, X. Chen, D. Chen, X. Zheng, Y. Gao, W. Fang, *Adv. Mater.* **2018***, 30,* 1801387.

[17] H. Zhang, S. Chen, X. W. Sun, *ACS Nano* **2017***, 12*, 697.

[18] B. R. Lee, J. C. Yu, J. H. Park, S. Lee, C. Mai, B. Zhao, M. S. Wong, E. D. Jung, Y. S. Nam, S. Y. Park, *ACS Nano* **2018***, 12*, 5826.

[19] W. K. Bae, J. Lim, D. Lee, M. Park, H. Lee, J. Kwak, K. Char, C. Lee, S. Lee, *Adv. Mater.* **2014***, 26*, 6387.

[20] M. K. Choi, J. Yang, K. Kang, D. C. Kim, C. Choi, C. Park, S. J. Kim, S. I. Chae, T. -H. Kim, J. H. Kim, T. Hyeon, D. -H. Kim, *Nat. Commun.* **2015**, *6*, 7149.

[21] H. Zhang, Q. Su, Y. Sun, S. Chen, *Adv. Optical Mater.* **2018**, *6*, 1800354.

[22] B. Li, M. Lu, J. Feng, J. Zhang, P. M. Smowton, J. I. Sohn, I. K. Park, H. Zhong, B. Hou, *J. Mater. Chem. C* **2020**, *8*, 10676.

[23] S. –Y. Yoon, J. –H. Kim, K. –H. Kim, C. –Y. Han, J. –H. Jo, D. –Y. Jo, S. Hong, J. Y. Hwang, Y. R. Do, H. Yang, *Nano Energy* **2019**, *63*, 103869.

[24] P. Shen, F. Cao, H. Wang, B. Wei, F. Wang, X. W. Sun, X. Yang, *ACS Appl. Mater. Interfaces* **2019**, *11*, 1065.

[25] B. S. Mashford, M. Stevenson, Z. Popovic, C. Hamilton, Z. Zhou, C. Breen, J. Steckel, V. Bulovic, M. Bawendi, S. Coe-Sullivan, P. T. Kazlas, *Nat. Photon.* **2013**, *7*, 407.

[26] H. Zhang, Q. Su, S. Chen, *Adv. Optical Mater.* **2020**, *8*, 1902092.

18

[27] Y. J. Choi, D. Hwang, H. Chung, D. Y. Kim, D. Kim, *NPG Asia Mater.* **2015**, *7*, e202.

[28] Y. Zhu, R. Xu, Y. Zhou, Z. Xu, Y. Liu, F. Tian, X. Zheng, F. Ma, R. Alsharafi, H. Hu, T. Guo, T. W. Kim, F. Li, *Adv. Optical Mater.* **2020**, *8*, 2001479.

[29] Y. Yuan, T. J. Reece, P. Sharma, S. Poddar, S. Ducharme, A. Gruverman, Y. Yang, J. Huang, *Nat. Mater.* **2011**, *10*, 296.

[30] Y. Cho, P. Giraud, B. Hou, Y. -W. Lee, J. Hong, S. Lee, S. Pak, J. Lee, J. E. Jang, S. M. Morris, J. I. Sohn, S. Cha, J. M. Kim, *Adv. Energy Mater.* **2018**, *8*, 1700809.

[31] M. N. Almadhoun, M. A. Khan, K. Rajab, J. H. Park, J. M. Buriak, H. N. Alshareef, *Adv. Electron. Mater.* **2019**, *5*, 1800363.

[32] A. Arrigoni, L. Brambilla, C. Bertarelli, G. Serra, M. Tommasini, C. Castiglioni, *RSC Adv.* **2020**, *10*, 37779.

[33] X. Zhao, H. Xuan, C. He, *RSC Adv.* **2015**, 5, 81115.

[34] Y. -Y. Choi, J. Hong, D. -S. Leem, M. Park, H. W. Song, T. -H. Sung, K. No, *J. Mater. Chem.* **2011**, *21*, 5057.

[35] Q. Du, J. Zheng, J. Wang, Y. Yang, X. Liu, *RSC Adv.* **2018**, *8*, 19585.

[36] J. Kim, J. H. Lee, H. Ryu, J. -H. Lee, U. Khan, H. Kim, S. S. Kwak, S. -W. Kim, *Adv. Funct. Mater.* **2017**, *27*, 1700702.

[37] J. -H. Lee, R. Hinchet, T. Y. Kim, H. Ryu, W. Seung, H. -J. Yoon, S. -W. Kim, *Adv. Mater.* **2015**, *27*, 5553.

[38] K. Y. Lee, S. K. Kim, J. -H. Lee, D. Seol, M. K. Gupta, Y. Kim, S. -W. Kim, *Adv. Funct. Mater.* **2016**, *26*, 3067.

19

[39] C. Xiang, L. Wu, Z. Lu, M. Li, Y. Wen, Y. Yang, W. Liu, T. Zhang, W. Cao, S. -W. Tsang, B. Shan, X. Yan, L. Qian, *Nat. Commun.* **2020**, *11*, 1646.

[40] A. Veamatahau, B. Jiang, T. Seifert, S. Makuta, K. Latham, M. Kanehara, T. Teranishi, Y. Tachibana, *Phys. Chem. Chem. Phys.* **2015**, *17*, 2850.

[41] X. Li, Y. -B. Zhao, F. Fan, L. Levina, M. Liu, R. Q. -Bermudez, X. Gong, L. N. Quan, J. Fan, Z. Yang, S. Hoogland, O. Voznyy, Z. -H. Lu, E. H. Sargent, *Nat. Photon.* **2018**, *12*, 159.33

[42] H. Moon, H. Chae, *Adv. Optical Mater.* **2020**, *8*, 1901314.

[43] W. Chen, X. Tang, P. Wangyang, Z. Yao, D. Zhou, F. Chen, S. Li, H. Lin, F. Zeng, D. Wu, K. Sun, M. Li, Y. Huang, W. Hu, Z. Zang, J. Du, *Adv. Optical Mater.* **2018**, *6*, 1800007.

[44] D. Hahm, J. H. Chang, B. G. Jeong, P. Park, J. Kim, S. Lee, J. Choi, W. D. Kim, S. Rhee, J. Lim, D. C. Lee, C. Lee, K. Char, W. K. Bae, *Chem. Mater.* **2019**, *31*, 3476.

[45] B. Hou, D. Parker, G. P. Kissling, J. A. Jones, D. Cherns, D. J. Fermín, *J. Phys. Chem. C* **2013**, *117*, 6814.

[46] D. Benito-Alifonso, S. Tremel, B. Hou, H. Lockyear, J. Mantell, D. J. Fermin, P. Verkade, M. Berry, M. C. Galan, *Angew. Chem. Int. Ed.* **2013**, *53*, 810.

[47] Y. Cho, B. Hou, J. Lim, S. Lee, S. Pak, J. Hong, P. Giraud, A. -R. Jang, Y. -W. Lee, J. Lee, J. E. Jang, H. J. Snaith, S. M. Morris, J. I. Sohn, S. Cha, J. M. Kim, *ACS Energy Lett.* **2018**, *3*, 1036.

[48] B. Hou, Y. Cho, B. S. Kim, J. Hong, J. B. Park, S. J. Ahn, J. I. Sohn, S. Cha, J. M. Kim, *ACS Energy Lett.* **2016**, *1*, 834.
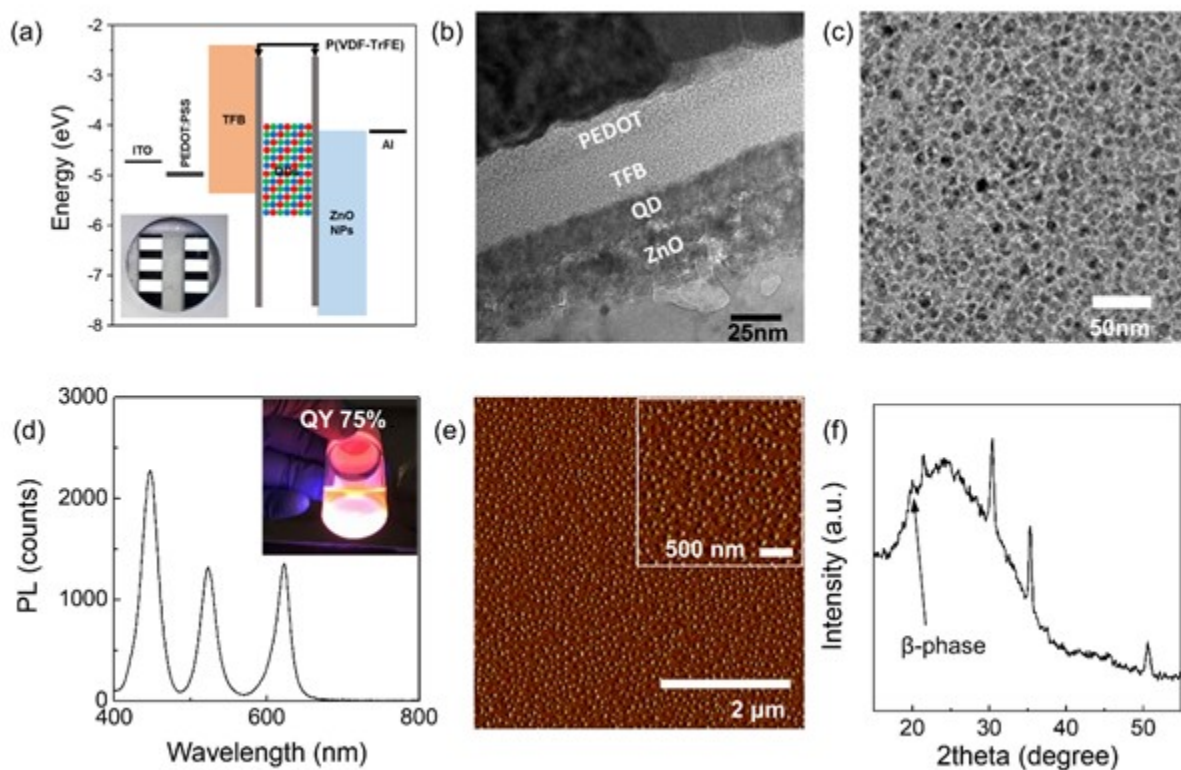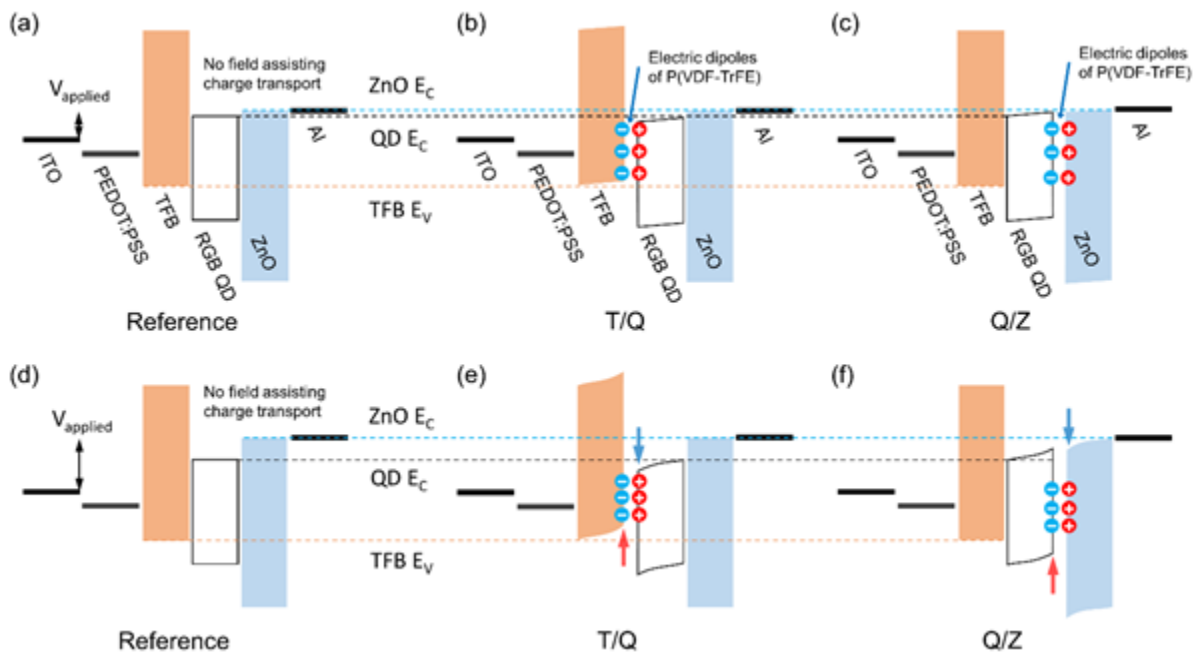
Figure 1. (a) Energy band diagram of the white FE-QLED without an applied bias. (b) TEM cross section image of the white FE-QLED. (c) TEM image of RGB mixed QDs. (d) PLQY of the RGB mixed QD solution where the inset shows the light emission of the mixed QDs under the UV light. (e) AFM image of the P(VDF-TrFE) islands layer on the QD film. (f) XRD patterns of FE-QLED.
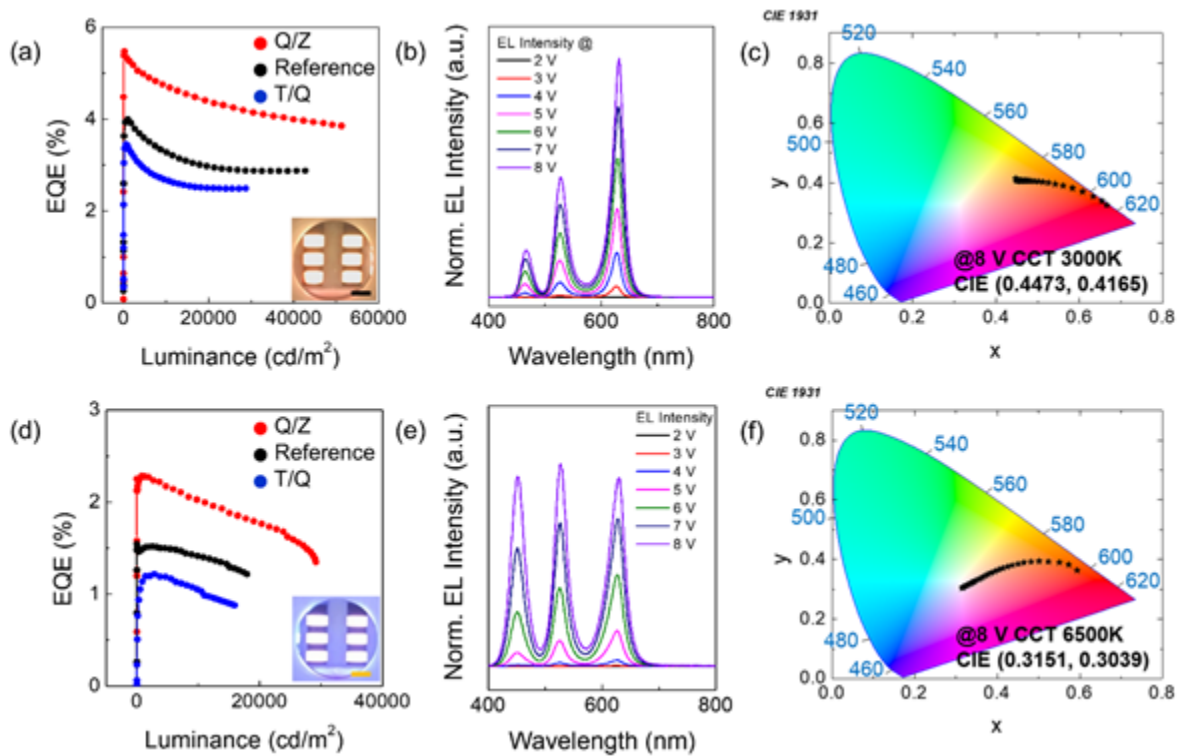
Figure 2. Energy band diagram of QLEDs for (a) a reference cell, (b) a T/Q cell, and (c) a Q/Z cell at low forward bias. (d)-(f) Energy band shift of QLEDs at high forward bias where (d), (e), and (f) corresponds to the devices shown in (a), (b), and (c), respectively. Negative and positive dipoles of P(VDF-TrFE) are depicted as blue and red circles in the figures.
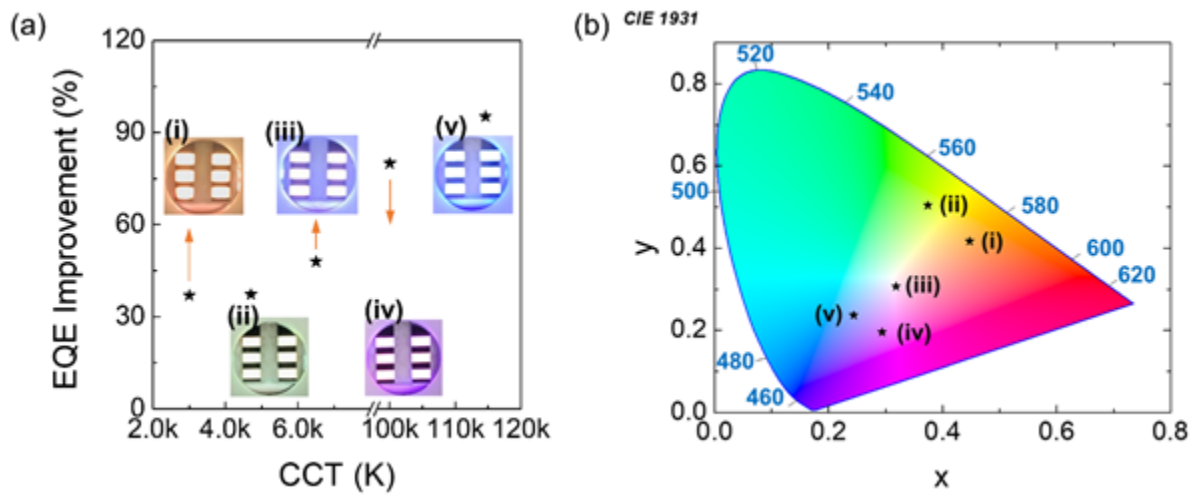
Figure 3. (a)-(c) Performance of warm white FE-QLED. (a) EQE as a function of Luminance, (b) EL spectra of FE-QLED and (c) CIE coordinate and CCT value of FE-QLED of the red line in Figure 3(a). (d)-(e) Performance of daylight white FE-QLED. (d) EQE as a function of Luminance, (e) EL spectra of FE-QLED and (f) CIE coordinate and CCT value of FE-QLED of the red line in Figure 3(d). The scale bar in (a) and (d) is 3 mm.

23

Figure 4. (a) CIE coordinates with respect to the FE-QLEDs with CCT values and corresponding digital images. (b) EQE improvement in FE-QLEDs with different CCT values using the P(VDF-TrFE) islands structure.

24

Table 1. Device characteristics of warm and daylight white QLEDs.

		Turn-on [V]	Max. Luminance [cdm^{-2}]	Max. EQE [%]	CCT [K]	CIE coordinate [x, y]	Avg. EQE[#] [%]
Warm white	T/Q[*]	2.0	28680	3.454	~2000	0.5263, 0.4071	3.28 ± 0.21
	Ref	2.0	42670	3.998	~2000	0.5242, 0.4092	3.91 ± 0.26
	Q/Z[**]	2.1	51220	5.476	~3000	0.4473, 0.4165	5.10 ± 0.35
Daylight white	T/Q[*]	2.6	15900	1.218	~25000	0.2404, 0.2630	1.07 ± 0.10
	Ref	2.6	17338	1.542	~19000	0.2490, 0.2686	1.41 ± 0.15
	Q/Z[**]	2.7	22710	2.284	~6500	0.3151, 0.3039	2.16 ± 0.12

[*]T/Q – ITO/ PEDOT:PSS/ TFB/ P(VDF-TrFE)/ QD/ Al

[**]Q/Z – ITO/ PEDOT:PSS/ TFB/ QD/ P(VDF-TrFE)/ Al

[#]Average EQE from 10 QLEDs of each type of the devices

Table of Contents
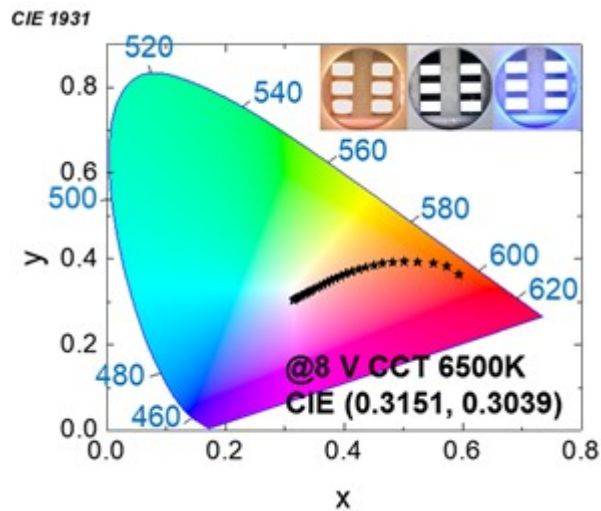
Short summary

Efficient direct white light emission has been a challenge due to inevitable energy band mismatch at interfaces between quantum dots with different bandgaps. The embedded ferroelectric island structure effectively modulates the energy band at the junction interface, and this leads to improved direct white light emission efficiency with various color temperatures.